Switchability Of A Single Port SAW Resonator Using The Electrical Bragg Band Gap

R. Alcorta Galván,[1, a)] C. Croënne,[1] B. Dubus,[1] B. Loiseaux,[2] E. Eustache,[2] M. Bertrand,[2] and A.-C. Hladky-Hennion[1]

[1)] *Univ. Lille, CNRS, Centrale Lille, Univ. Polytechnique Hauts-de-France, Junia, UMR 8520 - IEMN, F-59000 Lille, France*

[2)] *THALES Research & Technology France, Campus Polytechnique, 1 avenue Augustin Fresnel, F-91767 Palaiseau Cedex, France*

(Dated: 2 May 2022)

A proof of concept of a new solution for achieving tunable SAW components based on the Electrical Bragg band Gap concept developed for piezoelectric Phononic Crystals (PnCs) is presented on a SAW resonator on a $LiNbO_3$ substrate. In this work, it is shown that for a fixed geometry it is possible to shift the main resonance frequency by modifying the electrical condition on the electrodes that constitute the cavity's mirrors. The concept was validated by both numerical simulations and experimental characterization of single port resonators fabricated on $LiNbO_3$.

Phononic crystals (PnCs) may exhibit frequency ranges (band gaps) where propagation of elastic waves is prohibited. Mechanisms such as mode coupling[1], internal resonance[2] and Bragg scattering allow the formation of the band gap. Bragg mirrors, i.e. 1D PnCs, are extensively used in surface acoustic wave (SAW) devices to confine acoustic modes in a cavity, or to couple different cavities in specific frequency ranges. These devices exploit piezoelectric materials in order to couple acoustic waves and electrical signals, thus enabling their use for filtering applications in communication systems.

Band gap tunability of piezoelectric PnCs has already been the subject of numerous studies. Rupp et al.[3] have achieved switchable wave filtering and guiding, energy harvesting and actuating by placing electrodes on each side of a piezoelectric plate with an optimized polarization pattern. In a survey of the state of Phononic materials research[4], Ruzzene et al. present their own experimental findings on a periodic beam fitted with piezoelectric patches whose electrical states are either shunted or connected to a resistance.

Additionally, it has been shown that a stack of piezoelectric bars, separated by electrodes, poled along their thickness, exhibits a band gap that can be cancelled by a change in the electrical conditions applied on the electrodes[5,6]. A piezoelectric plate, poled along its thickness, with a grating of electrodes on its top and bottom surfaces, has also been considered. In this case, no band gap appears when the electrodes are grounded whereas a band gap appears when the electrodes are in open circuit[7]. Due to its reliance on a discontinuity of the electric field between successive cells, this band gap has been named electrical Bragg band gap (EBBG). The goal of this work is to showcase the use of the EBBG to allow the tunability of SAW devices which are intensively used in radio-frequency filters for their high rejection levels, low energy consumption and device compactness.

The main mechanisms used to confer tunability to SAW components until now are wavelength selection[8], perturbation of SAW boundary conditions[9–11] and perturbation of material properties[12–14]. Other works[15,16] focus on design of tunable circuits that don't modify the SAW devices.

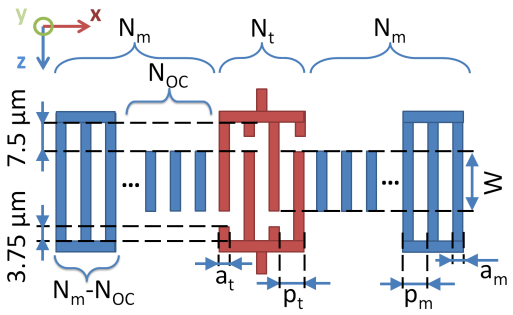

FIG. 1. Schematic description of the single-port resonator made of a transducer between two Bragg mirrors.

In this paper we propose to achieve switchable SAW components by changing the electrical conditions of periodic structures on the acoustic wave path. In particular a single port SAW resonator is considered (Fig. 1). The design of this type of resonator relies on a proper choice of different geometrical parameters: the period of the electrode array for the mirrors p_m and transducer p_t, the width of the electrodes a_m and a_t (or rather the corresponding fractions a_m/p_m and a_t/p_t), the thickness of the electrodes h, the number of fingers in the transducer N_t and the mirrors N_m, the distance between the transducer and the mirrors and finally the acoustic aperture of the device W (electrode length along z). Note that for the sake of simplicity this work focuses on symmetrical designs for the different electrical conditions on the mirrors and the distance between the transducers and mirrors is set to 0.

A certain number of the electrodes in the mirrors will be set to an open circuit condition (floating potential, also abbreviated as OC condition) while the rest will be connected to the electrical ground (this condition is abbreviated as GR condition). The number of open circuit electrodes in the mirrors is henceforth labeled N_{OC}. When $N_{OC} = 1$, the 2 electrodes closest to the transducer (one on each side) are switched (to an open circuit condition), when $N_{OC} = 2$, the 4 electrodes closest (two on each side) are set to an open circuit condi-

[a)] Electronic mail: ricardo.alcorta.g@gmail.com

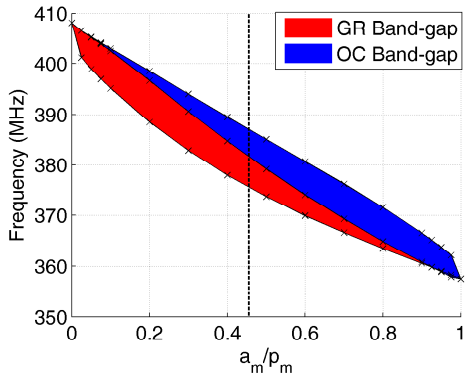

FIG. 2. Variations of the mirrors OC and GR band gaps as a function of the a_m/p_m ratio for p_m = 4.87 μm , h = 130 nm. Dashed line denotes the ratio $a_m/p_m = 0.455$

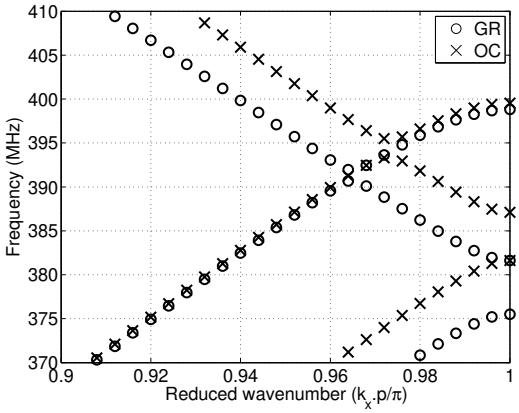

FIG. 3. Dispersion curves of the Bragg mirrors for the Rayleigh and SH SAW modes, for the GR and OC conditions, $a_m/p_m = 0.455$.

TABLE I. Geometrical Parameters of the Resonator.

	Period	a/p	Electrode thickness h	Number of electrodes
Transducer	4.74 μm	0.49	130 nm	17
Mirrors	4.87 μm	0.455	130 nm	72

tion and similarly for all values of N_{OC}. The floating potential electrodes are not connected to each other.

The Bragg band gaps for the Rayleigh mode of the infinite periodic grating with an infinite acoustic aperture over a semi-infinite substrate as a function of the ratio a_m/p_m and for both electrode connection schemes are calculated using finite element model (FEM) simulations, with the help of the ATILA code[17]. The substrate is $LiNbO_3$ with a YXl/128° cut. Metallizations are Au with a cubic crystalline structure. Further details of the model as well as the material constants used can be found in the supplementary materials.

Fig. 2 displays the band gaps for both the OC and GR conditions. The lower bound of the OC band gap is the upper bound of the GR band gap. The ratio $a_m/p_m = 0.455$ is chosen for the device under study. The OC band gap occurs in the [381.6, 387.1] MHz frequency range and the GR band gap in the [375.5, 381.6] MHz frequency range. The bandwidth being similar for both conditions, a similar reflection coefficient per period of the gratings is to be expected[18]. The geometrical parameters of the final device are presented in Table I, the acoustic aperture of the structure being $W = 200$ μm. To facilitate the switchable function by means of changes in the mirrors only, a relatively short transducer (17 electrodes) with low frequency selectivity is chosen (maximum of radiation conductance[19] for 380.2 MHz and a - 3 dB band between [368.9, 396.5] MHz).

In order to study the Bragg mirrors, the dispersion curves for the chosen geometry are calculated and shown in Fig. 3 for both connection schemes, namely grounded or floating electrodes. At the edge of the first Brillouin zone we can see the Bragg band gaps for the Rayleigh modes. As previously stated both gaps share one edge. For this mode, the field is anti-symmetric with a node in the center of the unit cell, and thus the potential under the electrode is null for both electrical conditions. Hybridization between the Rayleigh and SH-SAW modes also opens band gaps (as discussed by Zhang et al.[20]) in the [393.3, 395.4] MHz frequency range for the OC condition and in the [390.7, 392] MHz frequency range for the GR condition.

The design problem for this type of resonator is complexified by the presence of the transducer inside the cavity. Hashimoto et al.[21] treated this problem for transducers with significant internal reflections using the COM model and P-matrix representation. It was shown that when the mirror reflection coefficient is high enough (modulus close to 1) the resonator can be modeled as a Fabry-Perot cavity where the condition for resonance is set on the sum of the phase of the reflection coefficient of the mirrors and what can be seen as the acoustic transmission phase of the transducer (resulting from both propagation and the internal reflections). It is known that for the classical case (gratings all in GR or OC condition with a single Rayleigh mode) the reflection coefficient of a grating consists of a main lobe with high module and slowly varying phase, followed at higher and lower frequencies by lobes of decreasing magnitude and faster varying phase due to multiple reflections caused by the finite length of the grating. The center frequency of the main lobe is the center frequency of the band gap. Hence, main resonances occur in the resonator when the phase condition is met in or near the band gap. Additionally, the side lobes produce oscillations of the response since the phase condition may be met at their frequencies but the reflection coefficient has a lower amplitude. For mirrors with a higher number of electrodes the frequency range for the main lobe is narrow (its width approaching that of the band gap) and the reflection coefficient modulus is higher, whereas for lower numbers of electrodes the lobe broadens and the modulus is weaker. Finally, even though the COM model is the preferred tool to predict the electrical response of SAW resonators, it has been shown that deviations could appear for mirrors with a low number of electrodes[22], and thus a FEM model is more suited for our purposes.

In order to analyze the potential tunability of the resonator as a function of N_{OC}, simulations are to be carried out. As

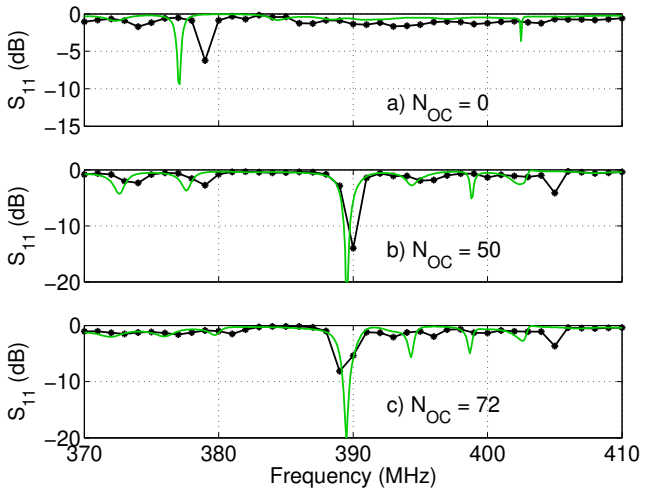

FIG. 4. Fit between the "slice model" (Green) and the full FEM simulation (Black) of the (a) $N_{OC} = 0$, (b) $N_{OC} = 50$ and (c) $N_{OC} = 72$ resonator by using a capacitance connected between each OC electrode and the ground.

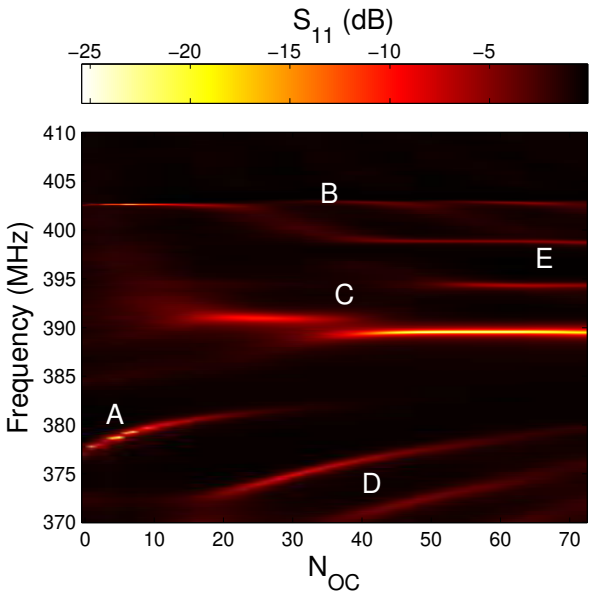

FIG. 5. S_{11} coefficient magnitude of the resonator (with the corrective capacitance) as a function of frequency and number of floating electrodes in each mirror N_{OC}. Port impedance is 50 Ω.

explained by Zhang et al.[20] coupling between the Rayleigh and SH modes can influence the propagation of the surface wave in the mirrors. Therefore a complete simulation of the cavity with its finite acoustic aperture must be carried out. This model is extremely demanding computationally. To reduce computational load, a simplified model was considered. Along the z direction, only a thin slice of the structure is considered, and a periodic boundary condition is set in order to simulate an infinite acoustic aperture case. It was found that undesirable differences between the two models frequency response exist. It was found heuristically that the electrical response of the resonator "slice" for cases with OC electrodes can be fitted to the one of the full device by artificially introducing an additional capacitance between each OC electrode and the electrical mass, no losses are added to either model. Fig. 4 shows a comparison between the two models for the $N_{OC} = 0$, $N_{OC} = 50$ and $N_{OC} = 72$ cases with the correction. For $N_{OC} = 0$ the correction can't be added since no floating potential electrodes are present, however for all cases the main resonances are present at reasonably close frequencies (2 MHz shift in the $N_{OC} = 0$ case and no shift for the $N_{OC} = 50$ and $N_{OC} = 72$ cases) and thus the "slice" model accurately enough represents the behaviour of the resonators to make qualitative statements on their working principles. Details on the value of the capacitance and the model are presented in the supplementary material.

Fig. 5 is a representation of the S_{11} coefficient magnitude for the resonator when the previously defined N_{OC} parameter is changed, calculated by the FEM using the COMSOL Multiphysics[23] software. This representation allows to track the evolution of the resonances as N_{OC} varies. The first column on the left shows the S_{11} spectrum for $N_{OC} = 0$. This is the configuration for which this resonator has been initially designed. A resonance due to the Rayleigh mode is present at 377.4 MHz, along with a secondary resonance at 402.4 MHz which corresponds to an SH-SAW cavity mode. With respect to this case, when N_{OC} is slightly increased, significant changes of the main resonance A appear, leading to visibly discontinuous evolutions of the S_{11} spectra. Since the "switched" electrodes are those closest to the transducer, one can generally expect stronger local effects in the few electrodes with OC conditions, positioned between the transducer and the rest of the electrodes with GR conditions. Capacitive coupling is also stronger between the transducer and the closest electrodes in the cavity. Closer inspection of the field maps for $N_{OC} = 3$ shows an example of these localized effects. In this case a group of OC electrodes with in-phase electric potential appears, causing important bulk acoustic wave radiation into the substrate and thus reducing the S_{11} parameter amplitude at resonance. As more electrodes are switched these highly localized effects tend to disappear. The resonance frequency is smoothly upshifted and the S_{11} parameter is degraded which implies a degradation of the magnitude of the effective reflection coefficient of the mirror and a phase change. In contrast, due to the low electro-mechanical coupling of the grating for this mode, the higher frequency SH-Rayleigh mode B of the cavity is barely affected by the changing number of OC electrodes. Mode C is the Rayleigh OC mode of the cavity, i.e. the main resonance when $N_{OC} = 72$. When $N_{OC} = 25$ the mode appears at a frequency slightly higher than that of the fully OC mirror and is thus a result of both the OC and GR parts of the mirror. When half the mirror is in OC condition ($N_{OC} = 36$), the slightly lower OC resonance appears and both merge as more electrodes are switched. For $N_{OC} > 50$ mode C is barely affected. At lower frequencies three streaks (labeled D) appear as more electrodes are switched and their frequencies shift smoothly with N_{OC}. They are attributed to ripples of the reflection coeffi-

cient due to the multiple reflections of the mirrors. Finally modes *E* that appear for higher numbers of OC electrodes in-between the SH and Rayleigh OC resonance frequencies are SH-Rayleigh hybrid modes of the cavity.

One can notice that either semi-continuous tunabilities or discrete jumps of the cavity resonances could be obtained by changing the electrical conditions on the mirrors. For instance, for low N_{OC} values mode *A* shifts of a few per thousands and modes *D* shift almost continuously. A jump of approximately 3% of the main resonance is obtained going from the GR condition to any N_{OC} value between 45 and 72. However, care must be taken as in some cases, oscillations of the S_{11} magnitude with frequency are comparable to the main resonance depth which is less than ideal for resonator operation. For example, for N_{OC} between 10 and 20 both *A* and *C* branches have a S_{11} parameter of comparable magnitude, not to mention the shear resonance *B* which is present throughout. On the other end of the graph, for the largest values of N_{OC}, not only the Rayleigh and SH but also the hybrid cavity modes strongly impact the S_{11} spectrum.

In order to verify the models experimentally a set of 5 devices is fabricated on a rectangular cut wafer. Resonators have been fabricated for 5 different N_{OC} values (N_{OC} = 0, 10, 30, 50, and 72) on a 4 inches $LiNbO_3$ YXl/128° substrate wafer with *Au* metallizations. A detailed representation of the metallization patterns is included in the supplementary materials. They were defined by e-beam lithography (Nanobeam Nb4 equipment) using a PMMA C7 resist. A 130 nm-thick layer of gold was then deposited by electron gun evaporation before the resist lift-off. The devices are vertically aligned to avoid longitudinal coupling between them. The resulting wafer cuts (on the *yz* plane) are not particularly sharp nor are parallel or perpendicular to the *x* or *y* axis in order to limit at the substrate edges, back reflections of surface waves leaking off the resonators. The electrical response of each sample is measured using a vector network analyser (VNA), coplanar Ground-Signal-Ground (GSG) probes and on-wafer calibration.

Fig. 6 presents the comparison between the "slice model" and experimental results for the five configurations. To account for deviations during the fabrication process 55 *nm* were taken from the width of each electrode in the simulations. Additionally it was found that adding losses of 1.185% to the dielectric tensor drastically improved the agreement between the measurements and simulation. The S_{11} coefficients for the simplified model are overall well correlated to the numerical results except for the $N_{OC} = 0$ case, for which a 2 MHz shift of the spectrum is observed. For this case the response for the complete resonator simulation for which the agreement is better is also shown. Small shifts for the rest of the cases can be attributed to various factors, such as the exact metallization layout or inaccuracies in the material parameters. Despite these inaccuracies, the jump of the main resonance is still present in the experimental measurements. Notably, relative frequency jumps of 2.88%, 2.9% and 3.19% can be seen between the $N_{OC} = 0$ case and the $N_{OC} = 72$, $N_{OC} = 50$ and $N_{OC} = 30$ cases respectively.

In this paper a 3% relative frequency shift of the main resonance of a one port SAW resonator through modification of the electrical conditions of its mirrors has been shown on FEM simulations. This frequency shift demonstrates the application of the EBBG for SAW component agility. The shift of the cavity resonance is a consequence of a variation of the effective reflection coefficient of the Bragg mirrors forming the cavity. The concept was validated by measurements made on "frozen" (i.e. constituted of electrodes permanently in open circuit or grounded) resonators with different numbers of floating potential electrodes. The next step is to introduce electrical switches in the design to allow controllable electrical conditions on the mirror electrodes.

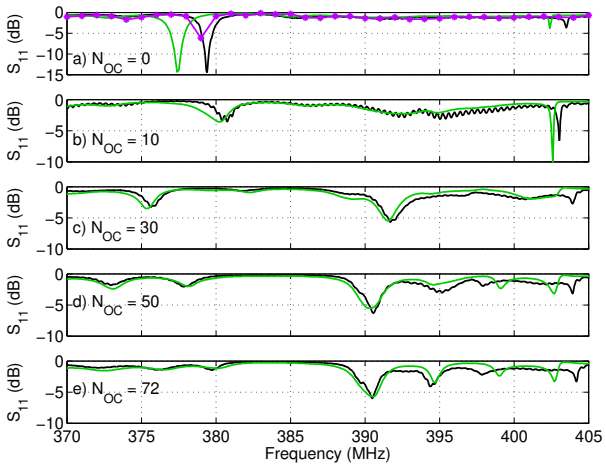

FIG. 6. Simulated (green) and measured (black) S_{11} magnitude spectra for resonators with N_{OC} = 0, 10, 30, 50, and 72. Port Impedance is 50 Ω. For the N_{OC} = 0 case, the complete resonator simulation is also shown (magenta).

Moreover, the resonator was initially designed in order to exhibit an optimized response when the electrodes of the Bragg mirrors are grounded without taking into account the resonator response once the electrodes are switched. Such an approach does not necessarily lead to an optimal solution in terms of tunability. To design SAW components with tunability in mind, optimisation tools using fast modelling methods such as the Mixed Matrix method[24] should be used on all the geometrical parameters of the device and the electrical conditions of the mirrors in order to obtain acceptable performance for all working points.

SUPPLEMENTARY MATERIAL

See supplementary material for details on the FEM model as well as the characterization and layout of the fabricated devices.

ACKNOWLEDGMENTS

The authors wish to thank Claude Prévot for the fruitful discussions and Stéphane Xavier for the electron-beam

lithography. This work was supported by the French Agence Nationale de la Recherche (FORMOSA project ANR-18-ASMA-0003-01), the Agence Innovation Défense, and the Région Hauts-de-France.

DATA AVAILABILITY STATEMENT

The data that support the findings of this study are available from the corresponding author upon reasonable request.

[1]N. Kherraz, L. Haumesser, F. Levassort, P. Benard, and B. Morvan, J. Appl. Phys. **123**, 094901 (2018).
[2]L. Airoldi and M. Ruzzene, New Journal of Physics **13**, 113010 (2011).
[3]C. J. Rupp, M. L. Dunn, and K. Maute, Appl. Phys. Lett. **96**, 111902 (2010).
[4]M. Hussein, M. Leamy, and M. Ruzzene, Appl. Mech. Rev. **66**, 040802 (2014).
[5]S. Degraeve, C. Granger, B. Dubus, J. Vasseur, M. P. Thi, and A.-C. Hladky-Hennion, J. Appl. Phys. **115**, 194508 (2014).
[6]M.-F. Ponge, B. Dubus, C. Granger, J. Vasseur, M. Pham Thi, and A.-C. Hladky-Hennion, IEEE Trans. Ultrason. Ferroelectr. Freq. Control. **62**, 1114–1121 (2015).
[7]C. Vasseur, C. Croënne, B. Dubus, J. Vasseur, A. Hladky-Hennion, C. Prévot, P. Martins, and M. Pham-Thi, in *2017 IEEE International Ultrasonics Symposium (IUS)* (2017) pp. 1–4.
[8]J. Zhu, N. W. Emanetoglu, Y. Lu, J. A. Kosinski, and R. A. Pastore, IEEE Trans. Ultrason. Ferroelectr. Freq. Control. **48, no. 5**, 1383–1388 (2001).
[9]R. Li, P. Reyes, S. Ragavendiran, H. Shen, and Y. Lu, Appl. Phys. Lett. **107**, 073504 (2015).
[10]R. Li, G. Li, W.-C. Hong, P. Reyes, K. Tang, K. Yang, S.-Y. Wang, H. Ye, Y. Li, L. Zhang, K. Kisslinger, and Y. Lu, Smart Mater. Struct. **27**, 085025 (2018).
[11]R. Li, P. Reyes, G. Li, K. Tang, K. Yang, S.-Y. Wang, J. Han, N. Emanetoglu, and Y. Lu, ECS J. Solid State Sci. Technol. **6**, S3119–S3124 (2017).
[12]H. Zhou, A. Talbi, N. Tiercelin, and O. Bou Matar, Appl. Phys. Lett. **104**, 114101 (2014).
[13]P. Smole, W. Ruile, C. Korden, A. Ludwig, E. Quandt, S. Krassnitzer, and P. Pongratz, in *Proc. IEEE Intl. Freq. Cont. Symp. 2003* (2003) pp. 903–906.
[14]S. Alzuaga, W. Daniau, R. Salut, T. Baron, S. Ballandras, and E. Defay, Appl. Phys. Lett. **105**, 062901 (2014).
[15]T. Wada, T. Ogami, A. Horita, H. Obiya, M. Koshino, M. Kawashima, and N. Nakajima, 2016 IEEE MTT-S Int. Microwave Symp. , 1–4 (2016).
[16]K. Hashimoto, T. Kimura, T. Matsumura, H. Hirano, M. Kadota, and M. Esashi, IEEE Microw. Mag. **16**, 89–97 (2015).
[17] (2010).
[18]V. Plessky and J. Koskela, Int. J. High Speed Electron. Syst. **10**, 867–947 (2000).
[19]G. Bu, D. Ciplys, M. Shur, L. Schowalter, S. Schujman, and R. Gaska, IEEE Trans. Ultrason. Ferroelectr. Freq. Control. **53**, 251–254 (2006).
[20]B. Zhang, T. Han, G. Tang, Q. Zhang, T. Omori, and K. Hashimoto, Jpn. J. Appl. Phys. **56**, 07JD02 (2017).
[21]K. Hashimoto, T. Omori, and M. Yamaguchi, IEEE Trans. Ultrason. Ferroelectr. Freq. Control.l **51**, 1394–1403 (2004).
[22]S. Lehtonen, V. Plessky, and M. Salomaa, IEEE Trans. Ultrason. Ferroelectr. Freq. Control. **51**, 343–351 (2004).
[23]S. COMSOL Multiphysics® v. 5.6. www.comsol.com. COMSOL AB, Stockholm,.
[24]P. Ventura, J. M. Hode, M. Solal, J. Desbois, and J. Ribbe, IEEE Trans. Ultrason. Ferroelectr. Freq. Control. **51, no. 11**, 1394–1403 (2004).
[25]N. Kherraz, L. Haumesser, F. Levassort, P. Benard, and B. Morvan, Appl. Phys. Lett. **108**, 093503 (2016).
[26]M. Rotter, A. Wixforth, W. Ruile, D. Bernklau, and H. Riechert, Appl. Phys. Lett. **73**, 2128–2130 (1998).
[27]S. Urabe, IEEE Trans. Ultrason. Ferroelectr. Freq. Control. **29, no. 5**, 255–260 (1982).
[28]J. Zhu, Y. Chen, G. Saraf, N. Emanetoglu, and Y. Lu, Appl. Phys. Lett. **89**, 103513 (2006).
[29]J. Pedrós, F. Calle, R. Cuerdo, J. Grajal, and Z. Bougrioua, Appl. Phys. Lett. **96**, 123505 (2010).
[30]D. Morgan, Electronics Letters **39**, 1361 – 1362 (2003).
[31]G. Kovacs, M. Anhorn, H. Engan, G. Visintini, and C. Ruppel, in *IEEE Symp. on Ultrason.*, Vol. 1 (1990) pp. 435–438.
[32]G. Kovacs, in *IEEE Symp. on Ultrason.*, Vol. 1 (2003) pp. 707–710.
[33]J. Koskela, V. Plessky, B. A. Willemsen, P. J. Turner, B. Garcia, R. B. Hammond, and N. O. Fenzi, in *2019 IEEE Int. Ultraso. Symp.(IUS)* (2019) pp. 181–184.
[34]M. Solal, IEEE Trans. Ultrason. Ferroelectr. Freq. Control. **50**, 1729–41 (2004).
[35]K. Hashimoto, *Surface Acoustic Wave Devices in Telecommunications: Modelling and Simulation* (Springer-Verlag Berlin Heidelberg GmbH, 2000).